JOURNAL OF COMPUTATIONAL PHYSICS 116, 330–342 (1995)

On the Time-Dependent Numerical Boundary Conditions of Magnetohydrodynamic Flows

M. T. SUN

Department of Mechanical Engineering, Chang Gung College of Medicine and Technology, Taoyuan, Taiwan

S. T. WU

Center for Space Plasma and Aeronomic Research and Department of Mechanical and Aerospace Engineering, The University of Alabama in Huntsville, Huntsville, Alabama 35899

AND

MURRAY DRYER

Space Environment Laboratory, National Oceanic and Atmospheric Administration, Boulder, Colorado 80303

Received May 20, 1993; revised April 15, 1994

The *time-dependent* numerical boundary conditions for time-dependent magnetodydrodynamic fluid flow simulations have been studied. In this paper, the formulation of the time-dependent numerical boundary conditions are described in a systematic way such that they can be adapted to different applications. In particular, the algorithm, which uses the boundary conditions for the solutions inside the computational domain of the test cases, is available for solving both parabolic and hyperbolic systems of partial differential equations. A numerical example for an astrophysical application in the context of photospheric shear induced dynamics is chosen to validate this new formulation. © 1995 Academic Press, Inc.

1. INTRODUCTION

Applications of numerical models in the field of astrophysics seek solutions of hyperbolic equations inside a finite domain with boundaries on which no physical boundary conditions can be specified. This approach is called the free boundary value problem. The method of characteristics is often used to specify numerically such boundary conditions in order to keep false physical properties from propagating into the domain as investigated by Wu and Wang [1].

Nakagawa *et al.* [2] developed the method of projected characteristics both to specify the numerical boundary conditions and to solve for the solutions in the computational domain. Hu and Wu [3] used the method for the numerical boundary conditions and developed the FICE (full-implicit-continuous-Eulerian) algorithm for the solutions inside the domain. The purpose of the present algorithm is to solve both parabolic and hyperbolic systems of equations. The algorithm used in the test run of this paper is a refined version of the FICE algorithm which has been renamed as the NICE (nimble implicit continuous-Eulerian) algorithm [4]. However, the method of projected characteristics requires complex formulation which may not be easily modified to suit different applications.

Thompson [5] extended the concept of non-reflecting boundary condtions to the multi-dimensional case in non-rectangular coordinate systems. He later developed a general boundary condition formalism [6] for all types of boundary conditions for first-order hyperbolic systems. However, these boundary conditions are limited to fluid dynamics. Vanajakshi *et al.* [7] then applied Thompson's method to solve boundary value problem in magnetohydrodynamics (MHD) particularly for isothermal plasma. Consequently, for non-isothermal plasma, the semi-analytic approach in solving numerically the eigenvectors of a modified version of the coefficient matrices is no longer valid.

In this paper, a new analytic approach is presented for non-isothermal plasma. In addition, when there are two eigenvectors that are parallel at a boundary, a special treatment is devised. The theoretical approach for this study is the same as that of Thompson's [6], namely, to systematize the formalism. Therefore, the readers are advised to consult Thompson's paper [6] for detailed characteristic analysis, nomenclature, and terminologies. In order to demonstrate the utility and accuracy of the present algorithm, numerical simulation for the dynamical evolution of a force-free mag-

0021-9991/95 $6.00

netic field is presented. These simulation results are compared with a set of quasi-static analytical solutions given by Martens *et al.* [8] for the accuracy test.

2. GOVERNING EQUATIONS

The normalized MHD equations for a perfectly conducting compressible fluid can be expressed in the vector form

$$\frac{\partial \rho}{\partial t} + \nabla \cdot (\rho \mathbf{v}) = 0, \tag{1}$$

$$\rho \frac{\partial \mathbf{v}}{\partial t} + \rho(\mathbf{v} \cdot \nabla)\mathbf{v} = -\frac{1}{\gamma M_0^2}\nabla p - \frac{2}{\beta_0 \gamma M_0^2}\mathbf{B} \times (\nabla \times \mathbf{B}) - \nabla \Phi, \tag{2}$$

$$\frac{\partial p}{\partial t} + (\mathbf{v} \cdot \nabla)p = -a^2 \rho \nabla \cdot \mathbf{v} + (\gamma - 1)\Delta Q, \tag{3}$$

$$\frac{\partial \mathbf{B}}{\partial t} = \nabla \times (\mathbf{v} \times \mathbf{B}), \tag{4}$$

where the equation of state $p = \rho T$ is used in the energy equation to replace ρT with pressure p. Φ is the stress tensor or the gravitational potential or both. ΔQ is the net rate of irreversible energy (heat) gain or loss per unit volume and a is the speed of sound. The two non-dimensional parameters, Mach number M_0 and plasma beta β_0, are expressed, respectively, as

$$M_0 = \frac{U}{a_0} = \frac{U}{\sqrt{\gamma R T_0}}, \quad \beta_0 = \frac{p_0}{B_0^2/8\pi},$$

where the constants subscripted with $(\,)_0$ are scaling factors for normalization purposes. Other scaling factors are $\rho_0 = p_0/RT_0$, x_0, v_0, and $t_0 = x_0/v_0$.

3. METHOD OF CHARACTERISTICS

For the convenience of using the method of characteristics on the boundary, the MHD equations need to be expressed as

$$\frac{\partial \mathbf{W}}{\partial t} + \mathbf{A}^{(1)}\frac{\partial \mathbf{W}}{\partial x_1} + \mathbf{A}^{(2)}\frac{\partial \mathbf{W}}{\partial x_2} + \mathbf{A}^{(3)}\frac{\partial \mathbf{W}}{\partial x_3} = \mathbf{E}. \tag{5}$$

The vector of primitive solution variables is

$$\mathbf{W}^{\mathrm{T}} = (\rho, u_1, u_2, u_3, p, B_1, B_2, B_3). \tag{6}$$

The 8×8 matrices are

$$\mathbf{A}^{(1)} = \frac{1}{h_1}$$

$$\begin{pmatrix} u_1 & \rho & 0 & 0 & 0 & 0 & 0 & 0 \\ 0 & u_1 & 0 & 0 & \frac{F_p}{\rho} & 0 & \frac{F_B}{\rho}B_2 & \frac{F_B}{\rho}B_3 \\ 0 & 0 & u_1 & 0 & 0 & 0 & -\frac{F_B}{\rho}B_1 & 0 \\ 0 & 0 & 0 & u_1 & 0 & 0 & 0 & -\frac{F_B}{\rho}B_1 \\ 0 & a^2\rho & 0 & 0 & u_1 & 0 & 0 & 0 \\ 0 & 0 & 0 & 0 & 0 & u_1 & 0 & 0 \\ 0 & B_2 & -B_1 & 0 & 0 & 0 & u_1 & 0 \\ 0 & B_3 & 0 & -B_1 & 0 & 0 & 0 & u_1 \end{pmatrix}, \tag{7}$$

$$\mathbf{A}^{(2)} = \frac{1}{h_2}$$

$$\begin{pmatrix} u_2 & 0 & \rho & 0 & 0 & 0 & 0 & 0 \\ 0 & u_2 & 0 & 0 & 0 & -\frac{F_B}{\rho}B_2 & 0 & 0 \\ 0 & 0 & u_2 & 0 & \frac{F_p}{\rho} & \frac{F_B}{\rho}B_1 & 0 & \frac{F_B}{\rho}B_3 \\ 0 & 0 & 0 & u_2 & 0 & 0 & 0 & -\frac{F_B}{\rho}B_2 \\ 0 & 0 & a^2\rho & 0 & u_2 & 0 & 0 & 0 \\ 0 & -B_2 & B_1 & 0 & 0 & u_2 & 0 & 0 \\ 0 & 0 & 0 & 0 & 0 & 0 & u_2 & 0 \\ 0 & 0 & B_3 & -B_2 & 0 & 0 & 0 & u_2 \end{pmatrix}, \tag{8}$$

$$\mathbf{A}^{(3)} = \frac{1}{h_3}$$

$$\begin{pmatrix} u_3 & 0 & 0 & \rho & 0 & 0 & 0 & 0 \\ 0 & u_3 & 0 & 0 & 0 & -\frac{F_B}{\rho}B_3 & 0 & 0 \\ 0 & 0 & u_3 & 0 & 0 & 0 & -\frac{F_B}{\rho}B_3 & 0 \\ 0 & 0 & 0 & u_3 & \frac{F_p}{\rho} & \frac{F_B}{\rho}B_1 & \frac{F_B}{\rho}B_2 & 0 \\ 0 & 0 & 0 & a^2\rho & u_3 & 0 & 0 & 0 \\ 0 & -B_3 & 0 & B_1 & 0 & u_3 & 0 & 0 \\ 0 & 0 & -B_3 & B_2 & 0 & 0 & u_3 & 0 \\ 0 & 0 & 0 & 0 & 0 & 0 & 0 & u_3 \end{pmatrix}, \tag{9}$$

where $a^2 = \gamma T$, $F_P = 1/(\gamma M_0^2)$, and $F_B = 2F_P/\beta_0$. The factor h_i is the scale length of the coordinate in the ith direction for the orthogonally curvilinear coordinate system. The vector of inhomogeneous terms is

$$\mathbf{E} = \begin{pmatrix} -\rho(\sum_{i=1,3}\sum_{j=1,3} u_i f_{ji} - \sum_{i=1,3} u_i f_{ii}) \\ \sum_{i=1,3}(u_i^2 - c_0 B_i^2) f_{i1} - \sum_{j=1,3}(u_1 u_j - c_0 B_1 B_j) f_{1j} - (\nabla\Phi)_1 \\ \sum_{i=1,3}(u_i^2 - c_0 B_i^2) f_{i2} - \sum_{j=1,3}(u_2 u_j - c_0 B_2 B_j) f_{2j} - (\nabla\Phi)_2 \\ \sum_{i=1,3}(u_i^2 - c_0 B_i^2) f_{i3} - \sum_{j=1,3}(u_3 u_j - c_0 B_3 B_j) f_{3j} - (\nabla\Phi)_3 \\ (\gamma - 1)\,\Delta Q - a^2\rho(\sum_{i=1,3}\sum_{j=1,3} u_i f_{ji} - \sum_{i=1,3} u_i f_{ii}) \\ u_1(B_1 f_{31} + B_2 f_{32} + B_3 f_{23}) + B_1(u_1 f_{21} + u_2 f_{12} + u_3 f_{13}) \\ u_2(B_1 f_{31} + B_2 f_{12} + B_3 f_{13}) + B_2(u_1 f_{21} + u_2 f_{32} + u_3 f_{23}) \\ u_3(B_1 f_{21} + B_2 f_{12} + B_3 f_{23}) + B_3(u_1 f_{31} + u_2 f_{32} + u_3 f_{13}) \end{pmatrix}, \quad (10)$$

where $c_0 = 2/(\gamma\rho M_0^2\beta_0)$ and

$$f_{ij} = \frac{1}{h_i} h_j \frac{\partial h_i}{\partial x_j}.$$

Equation (5) can also be rewritten as

$$\frac{\partial \mathbf{W}}{\partial t} + \mathbf{A}^{(1)}\frac{\partial \mathbf{W}}{\partial x_1} + \mathbf{C} = 0, \quad \mathbf{C} = \mathbf{A}^{(2)}\frac{\partial \mathbf{W}}{\partial x_2} + \mathbf{A}^{(3)}\frac{\partial \mathbf{W}}{\partial x_3} - \mathbf{E}. \quad (11)$$

The eight left eigenvectors $\mathbf{l}_i$ of $\mathbf{A}^{(1)}$ satisfy

$$\mathbf{l}_i^{\mathrm{T}}\mathbf{A}^{(1)} = \lambda_i^1 \mathbf{l}_i^{\mathrm{T}}, \quad i = 1, \ldots, 8, \quad (12)$$

where the eigenvalues λ_i^1 are given by

$$\det(\mathbf{A}^{(1)} - \lambda^1 \mathbf{I}) = 0. \quad (13)$$

A diagonalizing similarity transformation is generated for $\mathbf{A}^{(1)}$ by forming the matrix $\mathbf{S}_1$ such that its inverse $\mathbf{S}_1^{-1}$ has rows being the left eigenvectors $\mathbf{l}_i^{\mathrm{T}}$. The similarity transformation is

$$\mathbf{S}_1^{-1}\mathbf{A}^{(1)}\mathbf{S}_1 = \Lambda^1, \quad (14)$$

where Λ^1 is the diagonal matrix of the eigenvalues. Transforming Eq. (11) accordingly gives

$$\mathbf{S}_1^{-1}\frac{\partial \mathbf{W}}{\partial t} + \Lambda^1\mathbf{S}_1^{-1}\frac{\partial \mathbf{W}}{\partial x_1} + \mathbf{S}_1^{-1}\mathbf{C} = 0, \quad (15)$$

whose components are

$$\mathbf{l}_i^{\mathrm{T}}\frac{\partial \mathbf{W}}{\partial t} + \lambda_i^1\mathbf{l}_i^{\mathrm{T}}\frac{\partial \mathbf{W}}{\partial x_1} + \mathbf{l}_i^{\mathrm{T}}\mathbf{C} = 0, \quad i = 1, \ldots, 8. \quad (16)$$

For the reason of convenience, a vector $\mathscr{L}^1$ of components $\mathscr{L}_i^1$ is defined as

$$\mathscr{L}_i^1 \equiv \lambda_i^1\mathbf{l}_i^{\mathrm{T}}\frac{\partial \mathbf{W}}{\partial x_1}. \quad (17)$$

Equation (15) may now be written as

$$\mathbf{S}_1^{-1}\frac{\partial \mathbf{W}}{\partial t} + \mathscr{L}^1 + \mathbf{S}_1^{-1}\mathbf{C} = 0. \quad (18)$$

Then, appropriate boundary conditions, which are described in the next section in detail, are applied to specify the value of $\mathscr{L}_i^1$ for the inwardly pointing characteristic velocity λ_i^1 with respect to the solution volume; the rest of $\mathscr{L}_i^1$ are determined according to the definition in Eq. (17).

Now, multiply Eq. (18) by $\mathbf{S}_1$ giving

$$\frac{\partial \mathbf{W}}{\partial t} + \mathbf{S}_1\mathscr{L}^1 + \mathbf{C} = 0. \quad (19)$$

With the simple procedure of putting Eq. (19), for the definition of $\mathbf{C}$ back into Eq. (19), $\partial\mathbf{W}/\partial t$ is now completely defined. However, in order to solve for $\partial\mathbf{W}/\partial t$ in Eq. (19), the product $\mathbf{d}^1 \equiv \mathbf{S}_1\mathscr{L}^1$ is required with given $\mathbf{S}_1^{-1}$ and $\mathscr{L}^1$. Thus the system of equations

$$\mathbf{S}_1^{-1}\mathbf{d}^1 = \mathscr{L}^1 \quad (20)$$

have to be solved for $\mathbf{d}^1$.

At the position where three boundaries intersect, Eq. (10) becomes

$$\frac{\partial \mathbf{W}}{\partial t} + \mathbf{S}_1\mathscr{L}^1 + \mathbf{S}_2\mathscr{L}^2 + \mathbf{S}_3\mathscr{L}^3 - \mathbf{E} = 0. \quad (21)$$

Other than $\mathscr{L}^1$, $\mathscr{L}^2$ and $\mathscr{L}^3$ now also need to be taken care of by the boundary conditions. All of the following three sets of linear systems now need to be solved to obtain $\mathbf{d}^j$:

$$\mathbf{S}_j^{-1}\mathbf{d}_j = \mathscr{L}^j, \quad j = 1, 2, 3. \quad (22)$$

Back to Eq. (5), in the j direction, where $j = 1, 2, 3$, the eigenvalues of $\mathbf{A}^{(j)}$ are

$$\begin{gathered} \lambda_1^j = u_j, \quad \lambda_2^j = u_j, \quad \lambda_3^j = u_j + U_A^j, \\ \lambda_4^j = u_j - U_A^j, \lambda_5^j = u_j + U_f^j, \quad \lambda_6^j = u_j - U_f^j, \\ \lambda_7^j = u_j + U_s^j, \quad \lambda_8^j = u_j - U_s^j, \end{gathered} \quad (23)$$

where

$$U_A^j = |b_j|$$
$$(U_f^j)^2 = \tfrac{1}{2}(a^2 + b^2 + \sqrt{(a^2+b^2)^2 - 4a^2b_j^2}), \quad (24)$$
$$(U_s^j)^2 = \tfrac{1}{2}(a^2 + b^2 - \sqrt{(a^2+b^2)^2 - 4a^2b_j^2}).$$

The definition of b is

$$b_j \equiv \sqrt{F_B/\rho}\, B_j, \quad j = 1, 2, 3, \quad (25)$$

and

$$b^2 = \sum_{j=1}^{3} b_j b_j.$$

For simplicity, the following analysis is only in the x_1 direction. Details of the formulations in the other two directions are shown in the Appendix.

The inverse matrix $\mathbf{S}_1^{-1}$, whose rows are the left eigenvectors $\mathbf{l}_i^T$ of $\mathbf{A}^{(1)}$, which gives

$$\mathbf{S}_1^{-1} = \begin{pmatrix}
F_P a^2 & 0 & 0 & 0 & -F_P & 0 & 0 & 0 \\
0 & 0 & 0 & 0 & 0 & c_b & 0 & 0 \\
0 & 0 & -b_{13} & b_{12} & 0 & 0 & c_3 U_A^1 & -c_2 U_A^1 \\
0 & 0 & b_{13} & -b_{12} & 0 & 0 & c_3 U_A^1 & -c_2 U_A^1 \\
0 & U_f^1 u_{ff}^1 & -b_{12} U_f^1 & -b_{13} U_f^1 & F_P \dfrac{u_{ff}^1}{\rho} & 0 & c_2 u_f^1 & c_3 u_f^1 \\
0 & -U_f^1 u_{ff}^1 & b_{12} U_f^1 & b_{13} U_f^1 & F_P \dfrac{u_{ff}^1}{\rho} & 0 & c_2 u_f^1 & c_3 u_f^1 \\
0 & U_s^1 u_{ss}^1 & b_{12} U_s^1 & b_{13} U_s^1 & F_P \dfrac{u_{ss}^1}{\rho} & 0 & -c_2 u_s^1 & -c_3 u_s^1 \\
0 & -U_s^1 u_{ss}^1 & -b_{12} U_s^1 & -b_{13} U_s^1 & F_P \dfrac{u_{ss}^1}{\rho} & 0 & -c_2 u_s^1 & -c_3 u_s^1
\end{pmatrix}, \quad (26)$$

where $u_f^1 = (U_f^1)^2$, $u_s^1 = (U_s^1)^2$, $u_{ff}^1 = u_f^1 - b_1^2$, $u_{ss}^1 = b_1^2 - u_s^1$, $c_b = \sqrt{F_B/\rho}$, $c_i = c_b b_i$, and $b_{ij} = b_i b_j$. $\mathscr{L}^1$ can be calculated according to Eq. (17) and results in

$$\mathscr{L}^1 \equiv \Lambda_1 \mathbf{S}_1^{-1} \frac{\partial \mathbf{W}}{\partial x_1}, \quad (27)$$

or

$$\mathscr{L}_i^1 = \lambda_i^1 \sum_{k=1,8} \xi_{ik}^1 \frac{\partial W_k}{\partial x_1}, \quad (28)$$

where ξ_{ik}^1 is the element of $\mathbf{S}_1$ at row i and column k, and W_k is the kth element of $\mathbf{W}$. But the values of $\mathscr{L}_i^1$ for the inwardly pointing characteristic velocity λ_i^1 with respect to the solution volume are given according to appropriate boundary conditions which will be discussed in the next section.

Now $\mathbf{d}^1 = \mathbf{S}_1 \mathscr{L}^1$ can be solved with known $\mathbf{S}_1^{-1}$ and $\mathscr{L}^1$ through the set of equations

$$\mathbf{S}_1^{-1} \mathbf{d}^1 = \mathscr{L}^1. \quad (29)$$

Note that eigenvectors (left or right) of $\mathbf{A}^j$ will always be linearly independent, but they are not orthogonal, and it is possible that any two of them may be nearly parallel. Consequently the matrix $\mathbf{S}^{-1}$ may be ill-defined, because it is close to the vicinity of the singularity for which the numerical solution of Eq. (29) is poorly determined. In our case, this means $b_1 \to 0$. Therefore, Eq. (29) has to be solved analytically and the elements of the solution vector $\mathbf{d}^1$ in analytic form are

$$d_2^1 = \frac{\mathcal{M}_2/U_f^1 + \mathcal{M}_3/U_s^1}{2(u_f^1 - u_s^1)}, \quad (30)$$

$$d_3^1 = \frac{-U_f^1 b_3 \mathcal{M}_1 - b_2(\mathcal{M}_2 - 2\xi_{52}^1 d_2^1)}{2U_f b_1 (b_2^2 + b_3^2)}, \quad (31)$$

$$d_4^1 = \frac{U_f^1 b_2 \mathcal{M}_1 - b_3(\mathcal{M}_2 - 2\xi_{52}^1 d_2^1)}{2U_f b_1 (b_2^2 + b_3^2)}, \quad (32)$$

$$d_5^1 = \frac{\mathcal{N}_2/u_f^1 + \mathcal{N}_3/u_s^1}{2(\xi_{55}^1/u_f^1 + \xi_{75}^1/u_s^1)}, \quad (33)$$

$$d_6^1 = \mathscr{L}_2^1/\xi_{26}^1, \quad (34)$$

$$d_7^1 = \sqrt{\rho}\,\frac{\mathcal{N}_1 b_3 u_f^1 + b_2 U_A^1(\mathcal{N}_2 - 2\xi_{55}^1 d_5^1)}{2U_A^1 u_f^1 (b_2^2 + b_3^2)}, \quad (35)$$

$$d_8^1 = \sqrt{\rho}\,\frac{-\mathcal{N}_1 b_2 u_f^1 + b_3 U_A^1(\mathcal{N}_2 - 2\xi_{55}^1 d_5^1)}{2U_A^1 u_f^1 (b_2^2 + b_3^2)}, \quad (36)$$

$$d_1^1 = \frac{\mathscr{L}_1^1 - \xi_{15}^1 d_5^1}{\xi_{11}^1}, \quad (37)$$

where

$$\mathcal{M}_i = \sqrt{F_B}(\mathscr{L}_{2i+1}^1 - \mathscr{L}_{2i+2}^1), \quad (38)$$
$$\mathcal{N}_i = \mathscr{L}_{2i+1}^1 + \mathscr{L}_{2i+2}^1. \quad (39)$$

Note that d_i^1 are displayed in the solving order in which some of the solved elements may be used for solving the remaining unsolved elements.

In the case of $b_1 = 0$, then, this leads to any two eigenvectors being parallel and the analytical solution is not defined. Subconsequently $U_A^1 = 0$ and $U_s^1 = 0$. Physically, this means that the component of the magnetic induction normal to the boundary vanishes or the magnetic lines-of-force are parallel to the boundary. In this situation, a set of new eigenvectors needs to be sought. The determination of these new eigenvectors is described as follows:

Observing closely the original eigenvectors in the rows of $\mathbf{S}_1^{-1}$ in Eq. (26), one can see that l_1^T, l_2^T, l_5^T, and l_6^T still remain linearly independent to each other; i.e., they are still valid eigenvectors, while l_3^T, l_4^T, l_7^T, and l_8^T vanish. To find other valid eigenvectors, the original forms of the vanished eigenvectors are used in cooperation with the linearly combined eigenvectors, and then the limit $b_1 \to 0$ is taken. If l_3^T and l_4^T are summed and the resulting vector is scaled by $2U_A^1$, from which a valid eigenvector

$$l_3^T = (0, 0, 0, 0, 0, 0, c_b b_3, -c_b b_2) \tag{40}$$

can be derived. Scaling the summation of l_7^T and l_8^T with $2u_s^1$ and taking the limit $b_1 \to 0$, one gets another eigenvector,

$$l_7^T = (0, 0, 0, 0, F_P b^2/a^2\rho, 0, -c_b b_2, -c_b b_3). \tag{41}$$

Since the third and fourth components of all the eigenvectors available so far as zero, the most natural selections of the remaining two eigenvectors linearly independent to the other eigenvectors are

$$l_4^T = (0, 0, 1, 0, 0, 0, 0, 0), \quad l_8^T = (0, 0, 0, 1, 0, 0, 0, 0). \tag{42}$$

The new $\mathbf{S}_1^{-1}$ is now

$$\mathbf{S}_1^{-1} = \begin{pmatrix} F_P a^2 & 0 & 0 & 0 & -F_P & 0 & 0 & 0 \\ 0 & 0 & 0 & 0 & 0 & c_b & 0 & 0 \\ 0 & 0 & 0 & 0 & 0 & 0 & c_b b_3 & c_b b_2 \\ 0 & 0 & 1 & 0 & 0 & 0 & 0 & 0 \\ 0 & U_f^1 & 0 & 0 & F_P/\rho & c_b b_2 & c_b b_3 & 0 \\ 0 & -U_f^1 & 0 & 0 & F_P/\rho & c_b b_2 & c_b b_3 & 0 \\ 0 & 0 & 0 & 0 & F_P b^2/a^2\rho & -c_b b_2 & -c_b b_3 & 0 \\ 0 & 0 & 0 & 1 & 0 & 0 & 0 & 0 \end{pmatrix}. \tag{43}$$

The solution of Eq. (29) becomes

$$d_2^1 = \frac{\mathcal{L}_5^1 - \mathcal{L}_6^1}{2\xi_{52}^1}, \tag{44}$$

$$d_3^1 = \mathcal{L}_4^1/\xi_{43}^1, \tag{45}$$

$$d_4^1 = \mathcal{L}_8^1/\xi_{84}^1, \tag{46}$$

$$d_5^1 = \rho \frac{\mathcal{L}_5^1 + \mathcal{L}_6^1 + 2\mathcal{L}_7^1}{2F_P(1 + b^2/a^2)}, \tag{47}$$

$$d_6^1 = \mathcal{L}_2^1/\xi_{26}^1, \tag{48}$$

$$d_7^1 = \sqrt{\rho} \frac{b_3\mathcal{L}_3^1 + b_2(\mathcal{L}_5^1 + \mathcal{L}_6^1 - 2\xi_{55}^1 d_5^1)}{2b^2}, \tag{49}$$

$$d_8^1 = \sqrt{\rho} \frac{-b_2\mathcal{L}_3^1 + b_3(\mathcal{L}_5^1 + \mathcal{L}_6^1 - 2\xi_{55}^1 d_5^1)}{2b^2}, \tag{50}$$

$$d_1^1 = \frac{\mathcal{L}_1^1 - \xi_{15}^1 d_5^1}{\xi_{11}^1}. \tag{51}$$

After the above procedures are carried out in all three directions, the solutions $\mathbf{d}^1$, $\mathbf{d}^2$, and $\mathbf{d}^3$ are known. The time derivative of the primitive solution variables $\partial\mathbf{W}/\partial t$ can be calculated as

$$\frac{\partial \mathbf{W}}{\partial t} = -\mathbf{d}^1 - \mathbf{d}^2 - \mathbf{d}^3 + \mathbf{E}. \tag{52}$$

The time derivative is integrated through time with

$$\mathbf{W}(t + \Delta t) = \mathbf{W}(t) + \Delta t \frac{\partial \mathbf{W}}{\partial t} \tag{53}$$

to give the boundary values for a new time step. The NICE algorithm, then, utilizes the boundary values determined by the boundary condition to implicitly solve the variables inside the solution volume for the new time step.

4. BOUNDARY CONDITIONS OF MHD EQUATIONS

There are basically two different types of time-dependent boundary conditions that generally need to be treated with the characteristics method in the simulation of plasma phenomena.

The first type of boundary condition is the *non-reflecting boundary condition* which is commonly used when there is no physical boundary involved. Encountering this type of boundary in the problems of astrophysics is inevitable if the simulation domain is in a finite volume.

The second type of boundary condition is the *coupled boundary condition* which deals with boundaries at which only a portion of the physical properties is known. It is worth noting that, at any time t, the boundary conditions contribute only to the determination of $\partial\mathbf{W}/\partial t$ at the boundary, and never define $\mathbf{W}$ itself[6].

4.1. *Non-reflecting Boundary Conditions*

At the boundary $x_j = x_{j,\max}$, wave modes for which $\lambda_i^j > 0$ are propagating out of the computation and physical domain, and $\mathcal{L}_i^j$ may be computed from its definition in Eq. (17) using one-sided finite difference approximation to $\partial\mathbf{W}/\partial x_j$, using only interior data. (Similarly, at $x_j = x_{j,\min}$ we may compute $\mathcal{L}_i^j$ from its definition in Eq. (17) when $\lambda_i^j < 0$, using one-sided differences, as this case also corresponds to an outgoing wave.)

However, if $\lambda_i^j \leq 0$, then those waves are propagating into the computational and physical domain and generally may not

TABLE I

The Differencing Scheme for $\mathbf{W}_j^1$ and $\mathbf{W}_j^2$

Position	Value or differencing scheme	
x_j	$\mathbf{W}_j^1$ (backward)	$\mathbf{W}_j^2$ (forward)
$x_j = x_{j,\min}$	0	three point
$x_j = x_{j,\min} + \Delta x_j$	two point	three point
$(x_{j,\min} + \Delta x_j) < x_j < (x_{j,\max} - \Delta x_j)$	three point	three point
$x_j = x_{j,\max} - \Delta x_j$	three point	two point
$x_j = x_{j,\max}$	three point	0

be computed from interior data. In this case we make use of the non-reflecting boundary condition of Ref. [4] and set $\mathcal{L}_i^j = 0$ (and set $\mathcal{L}_i^j = 0$ at the inner boundary if $\lambda_i^j \geq 0$), which may be done conveniently by replacing λ_i^j by 0 or letting $\partial \mathbf{W}/\partial x_j$ be 0 in the definition of $\mathcal{L}_i^j$.

In the practical applications, two spatial derivatives denoted by $\mathbf{W}_j^1$ and $\mathbf{W}_j^2$ in each of the three directions ($j = 1, 2, 3$) are calculated at each boundary point. Both spatial derivatives are calculated using one-sided differencing: $\mathbf{W}_j^1$, backward differencing; $\mathbf{W}_j^2$, forward differencing. $\mathbf{W}_j^1$ is set equal to zero at the boundary points $x_j = x_{j,\min}$, evaluated with two-point differencing at the points $x_j = x_{j,\min} + \Delta x_j$ and evaluated with three-point differencing elsewhere. Likewise, $\mathbf{W}_j^2$ is set to zero at the boundary points $x_j = x_{j,\max}$, evaluated with two-point differencing at the points $x_j = x_{j,\min} - \Delta x_j$ and evaluated with three-point differencing elsewhere. The differencing scheme for these two spatial derivatives at different positions is summarized in Table I.

Then in Eq. (17), $\mathbf{W}_j^1$ is used in place of $\partial \mathbf{W}/\partial x_j$ when $\lambda_i^j \geq 0$ and $\mathbf{W}_j^2$ is used when $\lambda_i^j < 0$. This approach has one advantage over replacing λ_i^j with 0: because the stability and accuracy of the upwind scheme [9] in hyperbolic systems can be obtained.

4.2. *Coupled Boundary Conditions*

It is very difficult to give a general description of the boundary treatment for the coupled boundary conditions. Therefore, we have selected an example to illustrate the procedures of the treatment of the coupling boundary condition. In this numerical experiment, the normal direction of the boundary is in the x_3 direction which is z in the Cartesian coordinates. The experiment is done with symmetric conditions in the x_2 direction such that $\partial/\partial x_2 = 0$. The boundary conditions at $z = 0$ are $u_1 = u_3 = 0$, $u_2 = u_2(x_1, t)$, $\rho = \rho_0$, and $B_3 = B_3(x_1)$. Since the normal velocity $u_3 = 0$, the number of outgoing wave modes is three, which is the number of variables on the boundary needed to be determined. These variables are p, B_1, and B_2 for this particular example.

Equation (52), with $\mathbf{d}^2 = 0$, becomes

$$\frac{\partial \mathbf{W}}{\partial t} = -\mathbf{d}^1 - \mathbf{d}^3 + \mathbf{E}. \tag{54}$$

The known $\partial W_i/\partial t$, denoted by $(W_i)_t = 0$, are $(\rho)_t = 0$, $(u_1)_t = 0$, $(u_2)_t$, $(u_3)_t = 0$, and $(B_3)_t = 0$, whose indices are $i = 1, 2, 3, 4$, and 8, respectively. In the equation, $\mathbf{d}^1$ can be evaluated using Eq. (17) and the vector of inhomogeneous terms $\mathbf{E}$ can also be evaluated, assuming that the dissipation terms are either known or equal to zero at the boundary. Now $\mathcal{L}_i^3$, corresponding to the in-coming wave mode for which $\lambda_i^3 \geq 0$, must be evaluated such that the time derivatives can be treated as the known values.

We began with the solutions $\mathbf{d}^3$ of Eq. (54), such as

$$d_4^3 = \frac{\mathcal{M}_2/U_f^3 + \mathcal{M}_3/U_s^3}{2(u_f^3 - u_s^3)}, \tag{55}$$

$$d_2^3 = \frac{-U_f^3 b_2 \mathcal{M}_1 - b_1(\mathcal{M}_2 - 2\xi_{54}^3 d_4^3)}{2U_f b_3(b_1^2 + b_2^2)}, \tag{56}$$

$$d_3^3 = \frac{U_f^3 b_1 \mathcal{M}_1 - b_2(\mathcal{M}_2 - 2\xi_{54}^3 d_4^3)}{2U_f b_3(b_1^2 + b_2^2)}, \tag{57}$$

$$d_5^3 = \frac{\mathcal{N}_2/u_f^3 + \mathcal{N}_3/u_s^3)}{2(\xi_{55}^3/u_f^3 + \xi_{75}^3/u_s^3)}, \tag{58}$$

$$d_8^3 = \mathcal{L}_2^3/\xi_{28}^3, \tag{59}$$

$$d_6^3 = \sqrt{\rho}\,\frac{\mathcal{N}_1 b_2 u_f^3 + b_1 U_A^3(\mathcal{N}_2 - 2\xi_{55}^3 d_5^3)}{2U_A^3 u_f^3(b_1^2 + b_2^2)}, \tag{60}$$

$$d_7^3 = \sqrt{\rho}\,\frac{-\mathcal{N}_1 b_1 u_f^3 + b_2 U_A^3(\mathcal{N}_2 - 2\xi_{55}^3 d_5^3)}{2U_A^3 u_f^3(b_1^2 + b_2^2)}, \tag{61}$$

$$d_1^3 = \frac{\mathcal{L}_1^3 - \xi_{15}^3 d_5^3}{\xi_{11}^3}. \tag{62}$$

and the eigenvalues are

$$\lambda_1^3 = 0, \quad \lambda_2^3 = 0, \quad \lambda_3^3 = U_A^3, \quad \lambda_4^3 = -U_A^3, \lambda_5^3 = U_f^3, \quad \lambda_6^3 = -U_f^3, \quad \lambda_7^3 = U_s^3, \quad \lambda_8^3 = -U_s^3. \tag{63}$$

The components of $\mathcal{L}_i^3$ that need to be specified are $\mathcal{L}_1^3$, $\mathcal{L}_2^3$, $\mathcal{L}_3^3$, $\mathcal{L}_5^3$, and $\mathcal{L}_7^3$. From observation, one immediately noted that, by setting $(\rho)_t$ and $(B_3)_t = 0$, this procedure automatically determined $\mathcal{L}_1^3$ and $\mathcal{L}_2^3$, respectively. To determine the other three $\mathcal{L}_1^3$'s $\mathcal{M}_1$, $\mathcal{M}_2$, and $\mathcal{M}_3$ have to be solved from the simultaneous Eqs. (55), (56), and (57). The results are

$$\mathcal{M}_1 = 2b_3(b_1 d_3^3 - b_2 d_2^3), \tag{64}$$

$$\mathcal{M}_2 = -2U_f^3 b_3(b_1 d_2^3 + b_2 d_3^3) + 2U_f^3 d_4^3(U_f^2 - b_3^2), \tag{65}$$

$$\mathcal{M}_3 = U_s^3[2d_4^3(u_f^3 - u_s^3) - \mathcal{M}_2/U_f^3]. \tag{66}$$

where d_2^3, d_3^3, and d_4^3 can be obtained from

$$d_2^3 = e_2 - d_2^1 - (u_1)_t, \tag{67}$$

$$d_3^3 = e_3 - d_3^1 - (u_2)_t, \tag{68}$$

$$d_4^3 = e_4 - d_4^1 - (u_3)_t, \tag{69}$$

where e_i is the ith component of the vector of source terms **E**. Finally, we have

$$\mathcal{L}_3^3 = \mathcal{L}_4^3 + \frac{1}{\sqrt{F_B}}\mathcal{M}_1, \tag{70}$$

$$\mathcal{L}_5^3 = \mathcal{L}_6^3 + \frac{1}{\sqrt{F_B}}\mathcal{M}_2, \tag{71}$$

$$\mathcal{L}_7^3 = \mathcal{L}_8^3 + \frac{1}{\sqrt{F_B}}\mathcal{M}_3. \tag{72}$$

Now d_5^3, d_6^3, and d_7^3 can be determined from Eqs. (58), (60), and (61), respectively. Consequently, $(\mathrm{p})_t$, $(B_1)_t$, and $(B_2)_t$ are obtained from Eq. (54).

5. NUMERICAL EXPERIMENTS

The experiments are performed to verify the validity of the coupled and non-reflecting boundary conditions separately. The NICE algorithm has already been verified by the analytical solution of the Hartmann flow [4]. The physical problem of interest is the dynamic evolution of a magnetic force-free field driven by the shear motion of the foot points of the magnetic field lines.

In this scenario, we consider a force-free magnetic arcade straddling a photospheric neutral line. The arcade has translational symmetry along the neutral line, and rotational symmetry about an axis below the surface. In this Cartesian coordinate system, z denotes the height above the photosphere, x is the projected distance from the neutral line, and y is the coordinate normal to the x–z plane along the neutral line. A parameter t denotes the depth of the symmetry axis below the photosphere ($z < 0$).

One of the closed form analytical solutions for the physical scenario described above for the nonlinear force-free equation

$$\nabla \times \mathbf{B} = \alpha \mathbf{B} \tag{73}$$

obtained by Martens *et al.* [8] is

$$B_x = -B_0 z' \exp\left(\frac{t^2 - r^2}{2}\right) \tag{74}$$

$$B_y = -B_0 \sqrt{(1 - r^2)\exp(t^2 - r^2) + C^2} \tag{75}$$

$$B_z = B_0 x \exp\left(\frac{t^2 - r^2}{2}\right) \tag{76}$$

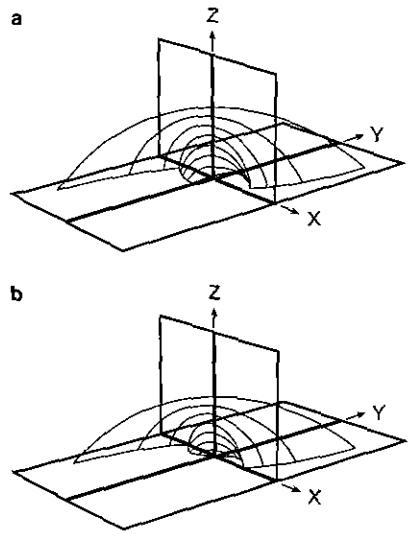

FIG. 1. Magnetic field configurations and displacement profiles for the photosphere with the parameters $C = 0.4$ and $t = 0$ in (a); $t = t_{\max}$ in (b).

$$\alpha = \frac{(2 - r^2)\exp\left(\frac{t^2 - r^2}{2}\right)}{\sqrt{(1 - r^2)\exp(t^2 - r^2) + C^2}}, \tag{77}$$

where $z' = z + t$ and $r^2 = x^2 + z'^2$. The foot point of a magnetic line-of-force has a shear displacement along a direction parallel to the neutral line given by

$$\Delta y(x, y, z = 0, t) = \tan^{-1}\left(\frac{x}{t}\right)\sqrt{1 - t^2 - x^2 + C^2\exp(x^2)}. \tag{78}$$

Velocity of the shear motion on the lower boundary of the computational domain can easily be obtained by the taking time derivative of the displacement in the above expression, Eq. (78), such that

$$v = \frac{-x}{t^2 + x^2}\sqrt{1 - t^2 - x^2 + C^2\exp(x^2)} - \tan^{-1}\left(\frac{x}{t}\right)\frac{t}{\sqrt{1 - t^2 - x^2 + C^2\exp x^2}}. \tag{79}$$

The time scale used in this numerical experiment is merely a parameter to describe the displacement of the foot points. The magnetic arcades and the displacement profiles on the photosphere are shown in Fig. 1 with the parameters $C = 0.4$ and in (a) $t = 0$ and in (b) $t = t_{\max} \equiv \sqrt{2 + 2\log C}$.

5.1. *Test One: Verification of the Coupled Boundary Condition*

To test the validity of the coupled boundary condition, two runs are carried out by using mathematical model equation (5)

with the same initial and upper and side boundary conditions, except that the boundary conditions at the lower boundary in each run are different. In run one, the lower boundary is specified with the known physical quantities. In run two, the coupled boundary condition in the previous section is used to calculate the physical quantities at the lower boundary. The results of the two runs are then compared to validate the coupled boundary condition.

In both runs, density, gas pressure, and temperature are kept constant at the lower boundary. The non-reflecting boundary conditions are used at the upper boundary and the two side boundaries, since there are the arbitrarily chosen boundaries and no physical boundary conditions can be specified on them. In one run, the lower boundary is specified with all of the magnetic induction components evaluated from the analytical solutions with $z = 0$ using Eqs. (74)–(76).

Initially, the atmosphere is isothermal and hydrostatic. The velocity field is described by

$$u = \frac{-zx}{x^2 + (z+t)^2} \tag{80}$$

$$v = \left[\frac{-x'}{t^2 + x'^2}\sqrt{1 - t^2 - x'^2 + C^2 e^{x'^2}} - \tan^{-1}\left(\frac{x'}{t}\right)\frac{t}{\sqrt{1 - t^2 - x'^2 + C^2 e^{x'^2}}}\right] \times \frac{|\arctan (z+t)/x| - \pi/2}{|\arctan t/x'| - \pi/2} \tag{81}$$

$$w = \frac{-z(z+t)}{x^2 + (z+t)^2}, \tag{82}$$

where $x' = \sqrt{(t+z)^2 + x^2 - t^2}$.

In this test, the simulation time period is equal to one-tenth of the maximum time and starts from zero, i.e., $0 \leq t \leq 0.041$ with $C = 0.4$. The physical parameters are listed in Table II. The domain size is 36 grid points by 25 grid points with the grid size $\Delta x = \frac{4}{25}$ and $\Delta z = \frac{1}{6}$. This makes the computational domain physical size 28,000 km in the x direction and 12,500 km in the z direction (height).

There are four monitored stations located at the grid points (19,10), (19,20), (30, 10), and (30, 20) as shown in Fig. 2. The first two stations are close to the neutral line and away from the lower boundary, at which the analytical solutions are specified as the boundary conditions. The second station is twice as far as the first station away from the lower boundary. The third and fourth stations are in the region away from the neutral line.

At these four monitored stations, the magnitude of the vector magnetic induction obtained from the numerical simulation is compared with that of the analytical solution. The relative errors of the comparison versus the time, normalized with the simulation period, are shown in Fig 3. for run one and Fig. 4 for run two, where the four frames show the comparisons at four different grid points as (a) point (19,10); (b) point (19,20); (c) point (30,10); and (d) point (30,20). Also in each frame, the results of three runs with different time steps are shown for the purpose of asymptotic analysis. The results from run one with 1000, 2000, and 5000 time steps in the simulation period are expressed in dash-dotted line, dashed line, and solid line, respectively. The reason for recording results with different time steps is to investigate the asymptotic behaviour of the solution, i.e., the time accuracy of the algorithm that solves the physical quantities in the computational domain. Since the results with 1000 time steps are close enough to the asymptotic solution with 5000 time steps, thus, the 1000 time steps are used for the number of time steps in run two. The dotted line is the two-degree polynomial least-square fitting of the curves of the error in each frame. These dotted lines indicate the center lines of the oscillating numerical results which deviate from the analytical solution by less than 2% for run one and 6% for run two.

TABLE II

Physical Parameters

Parameters	Numerical value	Unit
t_0	5000	s
L	5.0×10^8	cm
U	1.0×10^5	cm/s
γ	1.67	Dimensionless
R	1.653×10^8	erg/g-K
ρ_0	1.67×10^{-14}	g/cm^3
T_0	3.0×10^6	K
B_0	45	Gauss

From these results, it is easy to note that the waves propagating outward from the lower boundary in run two are elimintated. This indicates that the forced boundary condition at the lower boundary in run one creates spurious waves while the coupled boundary condition eliminates the spurious wave generation as demonstrated by run two. We may conclude that the coupled boundary condition is superior to the fixed boundary conditions.

At the region of monitored station (a), the deviation of the numerical results from the analytical solution becomes larger as time progresses. The end of the stimulation is *not* chosen purposely to avoid the growing deviation from the analytical solution, but is chosen randomly to be one-tenth of the characteristic time; i.e., the maximum time as discussed just prior to Section 5.1. The excessive decrease of the magnetic induction is caused by the convective effect of the dynamic system that brings in lower magnetic flux from a higher elevation through the convection process of a slightly over-predicted, downflowing velocity field, in comparison with analytical solutions. As for the other three monitored points, the gradients of the

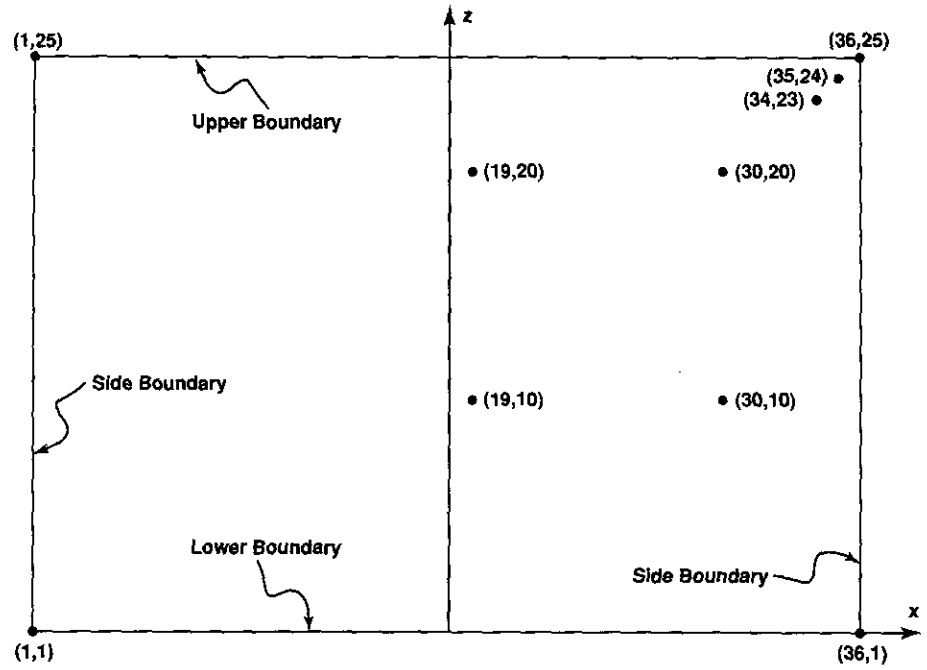

FIG. 2. The coordinate system and the locations of the monitored grid points for the experiments of the plasma shear flow.

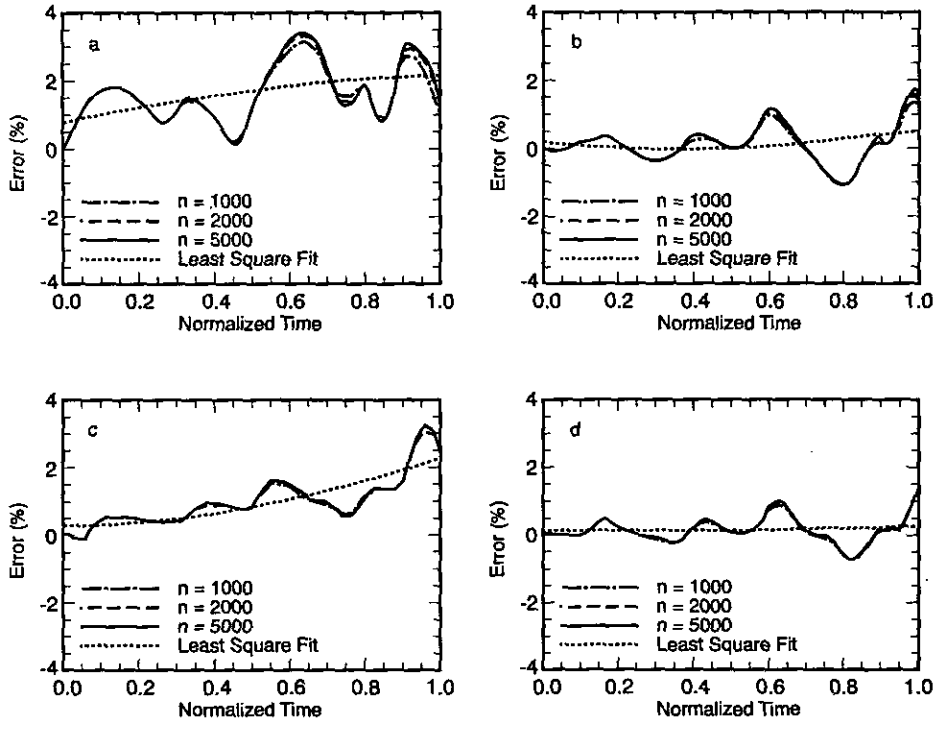

FIG. 3. The relative error of the magnitude of magnetic induction between numerical simulations and analytical solutions in run one (i.e., specified lower boundary conditions with known physical quantities) of test one at four monitored stations: (a) at (19,10); (b) at (19,20); (c) at (30,10); at (30,20), respectively, as shown in Fig. 2.

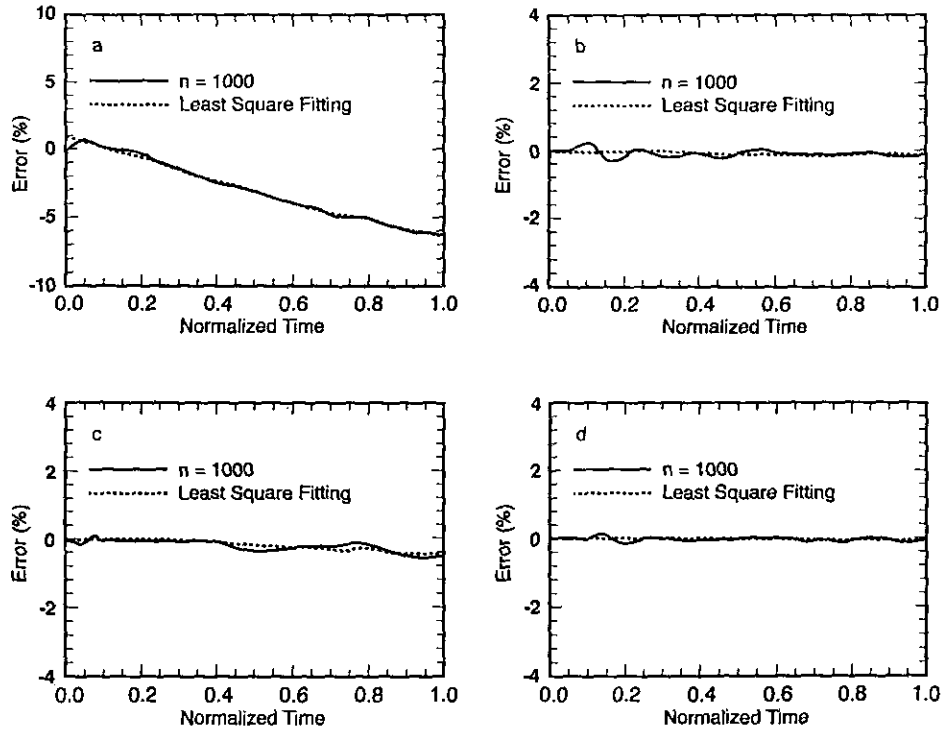

FIG. 4. The relative error of the magnitude of magnetic induction between numerical simulations and analytical solutions in run two (i.e., the quantities at the lower boundary are calculated according to the conditions discussed in (4.2)) of test one at four monitored stations: (a) at (19,10); (b) (19,20); (c) at (30,10); (d) at (30,20), respectively, as shown in Fig. 2.

magnetic induction in the vicinity of these points are not as large as at station (a). Therefore an over-predicted velocity field affects the magnetic flux very little through the convection process. However, this reflects the deviation of the dynamic simulation from the quasi-static solution, and the maximum deviation of the magnitude of the magnetic induction at monitored station (a) is around 6% at the end of the simulation.

5.2. *Test Two: Verification of the Non-reflecting Boundary Condition*

The non-reflecting boundary conditions are used in run one and run two of test one without verification because test one emphasizes the accuracy of the lower boundary. In test two the nonreflecting boundary conditions will be investigated. To carry out this test, all the parameters are the same as in run one of test one except that the domain size is larger, so that the boundary grid points, imposed with the non-reflecting boundary condition in run one of test one, become interior grid points in this test. Then the physical variables at these grid points, resulting from run one of test one are compared with those resulting from this test (i.e. test two) in order to verify the performance of the non-reflecting boundary conditions applied especially in the two-dimensional case. The reason for using this setup for run one of test one, instead of that of run two of test one, is that run one of test one creates waves which are considered to be undesired in a real simulation but which are useful for this test.

Since the positions of interest in this case are the intersections of non-reflecting boundaries, three monitored grid points are selected. The grid point (36,25) shown in Fig. 2, will be referred to as station (a) which is an intersecting point of two non-reflecting boundaries. The other two grid points (35,24) and (34,23) will be referred to as station (b) and station (c), respectively. These two stations are used to monitor the influence of the non-reflecting boundary condition on the interior grid points. The comparison of the results from run one of test one (shown by dotted lines) and the results from this test (in dashed lines) are shown in Fig. 5 and Fig. 6 with the three monitored stations in each figure. The two physical quantities compared are the normalized velocity component u in Fig. 5 and the normalized magnetic induction component B_y in Fig. 6. From these figures, the non-reflecting boundary condition is shown to work acceptably well in the multi-dimensional problem. However, we should point out that better approximations may exist, based on asymptotic analysis, when the far field is nearly uniform.

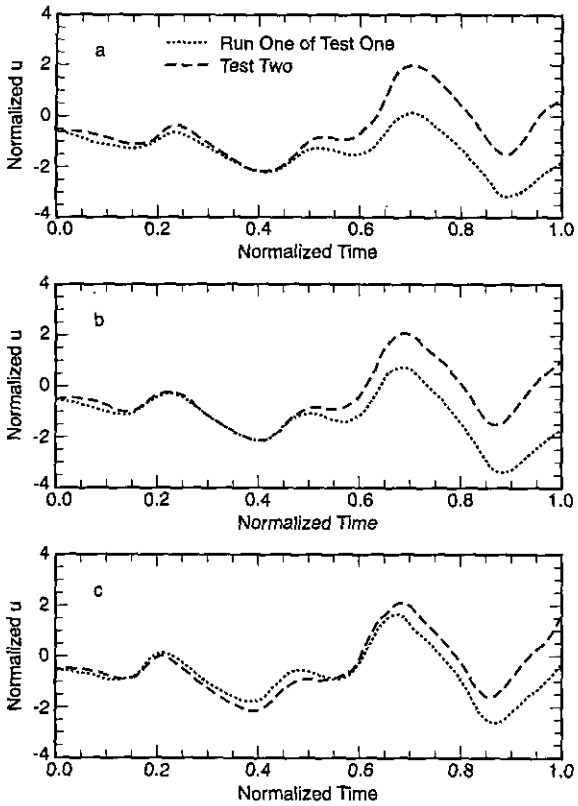

FIG. 5. Comparison of the normalized u resulting from run one of test one and test two at three monitored grid points: (a) at (36,25); (b) at (35,24); (c) at (34,23), respectively.

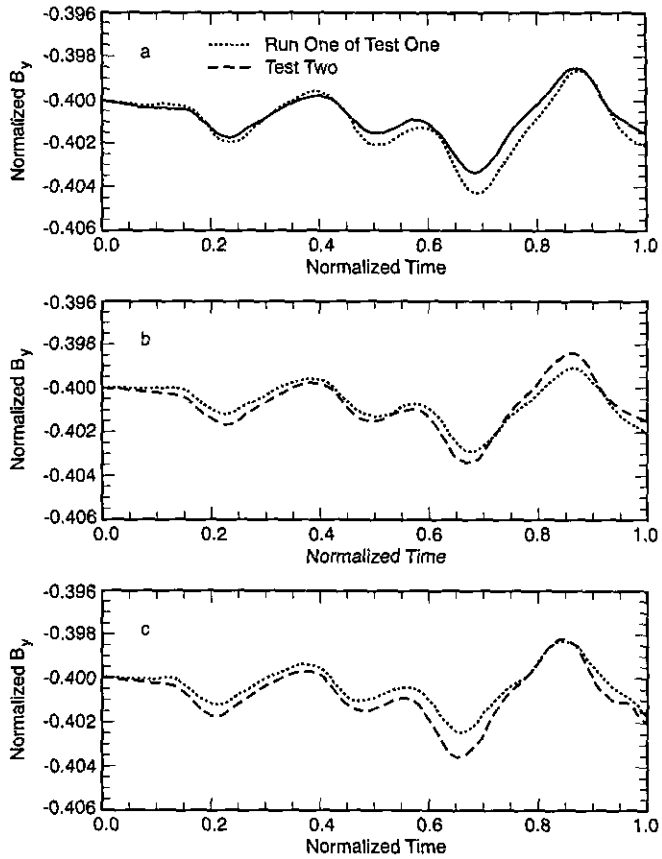

FIG. 6. Comparison of the normalized B_y resulting from run one of test one and test two at three monitored grid points: (a) at (36,25); (b) at (35,24); (c) at (34,23), respectively.

6. CONCLUSION

A new analytic approach of solving the time-dependent boundary conditions of MHD flow is developed for multi-dimensional non-isothermal plasma. In addition, for the situation when two of the eigenvectors are parallel, the solutions of the boundary conditions are shown to be achievable. Numerical experiments to test this formalism of the coupled boundary condition and the non-reflecting boundary condition are presented.

The test results of the coupled boundary condition show that the determination of $\partial \mathbf{W}/\partial t$ at the boundary is indeed much better than the artificially defined $\mathbf{W}$ (cf. [4]). This is especially true when the defined $\mathbf{W}$ is the solution of a set of steady state equations.

For the non-reflecting boundary condition, the test results demonstrate that the solutions on the upper and side boundaries in run one of test one act just like the solutions at the interior points in test two. The most troublesome point is the intersection of two non-reflecting boundaries which is one of the monitored points in the numerical experiment. This test proves the validity of the non-reflecting boundary condition in the multi-dimensional problem. The accuracy may be improved if the explicit determination of the boundary values can be formulated implicitly to the second-order accuracy compatible to the NICE algorithm. In such a case, the formulation will be much more complex than the present situation. This idea is one of our goals in the near future.

An application of this newly developed use of time-dependent boundary conditions can be found in the work of Martens *et al.* [8].

APPENDIX: Solutions of the Boundary Equations

In the x_2 direction, the inverse matrix $\mathbf{S}_2^{-1}$, whose rows are the left eigenvectors $\mathbf{l}_i^T$ of $\mathbf{A}^{(2)}$, is

$$\mathbf{S}_2^{-1} = \begin{pmatrix} F_P a^2 & 0 & 0 & 0 & -F_P & 0 & 0 & 0 \\ 0 & 0 & 0 & 0 & 0 & 0 & c_b & 0 \\ 0 & -b_{23} & 0 & b_{12} & 0 & c_3 U_A^2 & 0 & -c_1 U_A^2 \\ 0 & b_{23} & 0 & -b_{12} & 0 & c_3 U_A^2 & 0 & -c_1 U_A^2 \\ 0 & -b_{12} U_f^2 & U_f^2 u_{ff}^2 & -b_{23} U_f^2 & F_P \dfrac{u_{ff}^2}{\rho} & c_1 u_f^2 & 0 & c_3 u_f^2 \\ 0 & b_{12} U_f^2 & -U_f^2 u_{ff}^2 & b_{23} U_f^2 & F_P \dfrac{u_{ff}^2}{\rho} & c_1 u_f^2 & 0 & c_3 u_f^2 \\ 0 & b_{12} U_s^2 & U_s^2 u_{ss}^2 & b_{23} U_s^2 & F_P \dfrac{u_{ss}^2}{\rho} & -c_1 u_s^2 & 0 & -c_3 u_s^2 \\ 0 & -b_{12} U_s^2 & -U_s^2 u_{ss}^2 & -b_{23} U_s^2 & F_P \dfrac{u_{ss}^2}{\rho} & -c_1 u_s^2 & 0 & -c_3 u_s^2 \end{pmatrix}, \tag{83}$$

where $u_f^2 = (U_f^2)^2$, $u_s^2 = (U_s^2)^2$, $u_{ff}^2 = u_f^2 - b_2^2$, $u_{ss}^2 = b_2^2 - u_s^2$, $c_b = \sqrt{F_B/\rho}$, $c_i = c_b b_i$, and $b_{ij} = b_i b_j$. The elements of the solution vector $\mathbf{d}^2$ are

$$d_3^2 = \frac{\mathcal{M}_2/U_f^2 + \mathcal{M}_3/U_s^2}{2(u_f^2 - u_s^2)}, \tag{84}$$

$$d_2^2 = \frac{-U_f^2 b_3 \mathcal{M}_1 - b_1(\mathcal{M}_2 - 2\xi_{53}^2 d_3^1)}{2U_f^2 b_2(b_1^2 + b_3^2)}, \tag{85}$$

$$d_4^2 = \frac{U_f^2 b_1 \mathcal{M}_1 - b_3(\mathcal{M}_2 - 2\xi_{53}^2 d_3^1)}{2U_f^2 b_2(b_1^2 + b_3^2)}, \tag{86}$$

$$d_5^2 = \frac{\mathcal{N}_2/u_f^2 + \mathcal{N}_3/u_s^2}{2(\xi_{55}^2/u_f^2 + \xi_{75}^2/u_s^2)}, \tag{87}$$

$$d_7^2 = \mathcal{L}_2^{\xi_{27}^2}/\xi_{27}^2 \tag{88}$$

$$d_6^2 = \sqrt{\rho}\frac{\mathcal{N}_1 b_3 u_f^2 + b_1 U_A^2(\mathcal{N}_2 - 2\xi_{55}^2 d_5^2)}{2U_A^2 u_f^2(b_1^2 + b_3^2)}, \tag{89}$$

$$d_8^2 = \sqrt{\rho}\frac{-\mathcal{N}_1 b_1 u_f^2 + b_3 U_A^2(\mathcal{N}_2 - 2\xi_{55}^2 d_5^2)}{2U_A^2 u_f^2(b_1^2 + b_3^2)}, \tag{90}$$

$$d_1^2 = \frac{\mathcal{L}_1^2 - \xi_{15}^2 d_5^2}{\xi_{11}^2}, \tag{91}$$

where

$$\mathcal{M}_i = \sqrt{F_B}(\mathcal{L}_{2i+1}^2 - \mathcal{L}_{2i+2}^2), \tag{92}$$

$$\mathcal{N}_i = \mathcal{L}_{2i+1}^2 + \mathcal{L}_{2i+2}^2. \tag{93}$$

In the x_3 direction, the inverse matrix $\mathbf{S}_3^{-1}$, whose rows are the left eigenvectors $\mathbf{l}_i^T$ of $\mathbf{A}^{(3)}$, is

$$\mathbf{S}_3^{-1} = \begin{pmatrix} F_P a^2 & 0 & 0 & 0 & -F_P & 0 & 0 & 0 \\ 0 & 0 & 0 & 0 & 0 & 0 & 0 & c_b \\ 0 & -b_{23} & b_{13} & 0 & 0 & c_2 U_A^3 & -c_1 U_A^3 & 0 \\ 0 & b_{23} & -b_{13} & 0 & 0 & c_2 U_A^3 & -c_1 U_A^3 & 0 \\ 0 & -b_{13} U_f^3 & -b_{23} U_f^3 & U_f^3 u_{ff}^3 & F_P \dfrac{u_{ff}^3}{\rho} & c_1 u_f^3 & c_2 u_f^3 & 0 \\ 0 & b_{13} U_f^3 & b_{23} U_f^3 & -U_f^3 u_{ff}^3 & F_P \dfrac{u_{ff}^3}{\rho} & c_1 u_f^3 & c_2 u_f^3 & 0 \\ 0 & b_{13} U_s^3 & b_{23} U_s^3 & U_s^3 u_{ss}^3 & F_P \dfrac{u_{ss}^3}{\rho} & -c_1 u_s^3 & -c_2 u_s^3 & 0 \\ 0 & -b_{13} U_s^3 & -b_{23} U_s^3 & -U_s^3 u_{ss}^3 & F_P \dfrac{u_{ss}^3}{\rho} & -c_1 u_s^3 & -c_2 u_s^3 & 0 \end{pmatrix}, \tag{94}$$

where $u_f^3 = (U_f^3)^2$, $u_s^3 = (U_s^3)^2$, $u_{ff}^3 = u_f^3 - b_3^2$, and $u_{ss}^3 = b_3^2 - u_s^3$. The solution vector $\mathbf{d}^3$ is given in Section 4.2.

ACKNOWLEDGMENTS

The authors thank Dr. P. E. Martens for his invaluable comments and ideas. Thanks are due to Dr. K. W. Thompson for giving instructive suggestions during the period of this work. We also thank the referees for their constructive suggestions. It is also our pleasure to acknowledge that this work was supported in part by NASA Headquarters under Grant NAGW-9 and NOAA (*50RANR000104*). In addition, partial support from *NSPO/Taiwan/ROC* is also acknowledged.

REFERENCES

1. S. T. Wu and J. F. Wang, *Comput. Methods Appl. Mech. Eng.* **64,** 267 (1987).
2. Y. Nakagawa, Y. Q. Hu, and S. T. Wu, *Astron. Astrophys.* **179,** 354 (1987).
3. Y. Q. Hu and S. T. Wu, *J. Comput. Phys.* **55,** 33 (1984).
4. M. T. Sun, Ph.D. dissertation, University of Alabama in Huntsville, 1991.
5. K. W. Thompson, *J. Comput. Phys.* **68,** 1 (1987).
6. K. W. Thompson, *J. Comput. Phys.* **89,** 439 (1990).
7. T. C. Vanajakshi, K. W. Thompson, and D. C. Black, *J. Comput. Phys.* **84,** 343 (1989).
8. P. Martens, M. T. Sun, and S. T. Wu, *Eruptive Solar Flares,* edited by Z. Svestka, B. V. Jackson, and M. Machado, IAU Symposium 133, Igazu, Argentina, August 2–6, 1991 (Springer Verlag, New York/Berlin, 1992), p. 65.
9. S. V. Patankar, *Numerical Heat Transfer and Fluid Flow* (Hemisphere, Washington, DC, 1980).